Gold Nanorod Growth and Etching Activated by Femtosecond Irradiation and Surface Plasmon Resonance

Adem Dahi, Arnaud Rogemont, Yoann Brûlé, Christophe Labbez, Remi Chassagnon, Aurélien Coillet, Erik Dujardin, Julien Boudon, Benoît Cluzel

Gold nanorods growth and etching activated by femtosecond irradiation and Surface Plasmon Resonance

Adem Dahi, Arnaud Rogemont, Yoann Brûlé, Christophe Labbez, Remi Chassagnon, Aurélien Coillet, Erik Dujardin, Julien Boudon, and Benoît Cluzel*

Laboratoire Interdisciplinaire Carnot de Bourgogne, UMR CNR 6303, Université de Bourgogne, 9, Avenue Alain Savary, 21078 Dijon, France

E-mail: Benoit.Cluzel@u-bourgogne.fr

Abstract

Metal nanoparticle colloids provide a unique combination of optical, magnetic, electronic and thermal properties finding applications in various fields ranging from optoelectronics to cancer therapy. Chemical synthesis of such nanoparticles has been refined to a high degree of control of crystallinity, shape and size distribution. Among them, gold nanoparticles are of particular interest because they host plasmonic resonances that enhance their interactions with light. Their size and shape imposes the resonance wavelengths which, depending on the application, must be tunable. For this, the synthesis processes are generally adapted on a case-by-case basis, preventing the development of a generic recipe that can cover a wide range of applications. We present here a different approach and propose to modify the size distribution of post-synthesis nanoparticles by laser irradiation in the presence of a gold salt to tune their resonance wavelengths. Plasmonic resonances driven by femtosecond laser irradiation are used to tune the redox activity of $AuCl_4^-$ ions in the presence of gold nanorods which leads to

a reshaping of nanoparticles. All chemical intermediates and products are monitored by *in situ* UV-visible spectroscopy, ex-situ electronic microscopy analysis, and then compared to 3D simulations in order to unveil the underlying photochemical processes. As such, these results not only pave the way for the fine tuning of the plasmon resonance of gold colloids over a wide spectral range, which can have an impact on many application areas such as plasmonic colours, sensors or absorbers but also feeds into the very active field of plasmonic photocatalysis.

Introduction

Gold nanoparticles (NP) and nanoantennae have attracted a sustained interest because of their remarkable optical, thermal and electronic properties which results from the interaction between the collective oscillations of electrons at the dielectric-metal interface under an incident electromagnetic field. The properties associated with these localized surface plasmon resonances - namely resonance wavelengths, radiation patterns and field enhancement - are mainly governed by the shape of the nanoparticles, which must be precisely controlled. Thus, plasmonic resonator nanoantennae nanofabricated from sputtered gold films by planar lithographic technologies are produced with a high degree of control of morphology and on-chip integration. However, this top-down approach is hardly upscalable. On the contrary, chemical synthesis of metal nanoparticles has been refined to a high degree of control of crystallinity, size tunability and narrow size distribution. Even though a growing ensemble of morphologies are achievable, the shapes of crystalline nanoparticles is, to a large extent, determined by the symmetry properties of the underlying crystal.[1,2] To circumvent this limitation, several recently developed post-synthesis methods propose to modify the morphology of already synthesized colloid through etching[3–5] or overgrowth of the NP.[5–8]

Among the different shapes available by colloidal synthesis, gold nanorods (NR) are of particular interest since they exhibit two independant resonant modes lying in the visible and near infrared spectral range. The transverse surface plasmon resonance (TSPR) occurs

just above 500 nm and exhibits low dependence on morphology, while the longitudinal surface plasmon resonance (LSPR) occurs at higher wavelengths and is highly sensitive to the morphology. In many fields, such as biosensing, harmonic generation, optoelectronic conversion, that exploit phenomena directly related to the energy-specific optical excitation of the LSPR, a strict control of the Au NR aspect ratio (AR) and, in practice, of its length is a requirement. During seed-mediated NR synthesis, the most commonly adopted method, the final AR primarily depends on several parameters. The size (1 nm to 5 nm) and twinning state of the nuclei formed by the reduction of tetrachloroauric acid ($AuCl_4^-$) in presence of a stabilizing agent for (100) atomic planes, usually cetyltrimethylammonium bromide (CTAB), will set the fraction of NR among all possible morphologies. These nuclei are then added, as seeding centers, in a growth solution composed, at least, of $AuCl_4^-$, a (100)-facet stabilizing agent such as CTAB and a mild reducing agent that converts Au(III) into Au(I) but not into Au(0). The chemical composition of the growth solution and the reaction time and temperature govern the relative kinetics of the length vs diameter growth and thus the final AR distribution. Slight variations in these parameters affect significantly the resulting NR sizes and morphology.[9–12] Therefore, achieving fine tuning of the LSPR through seed-mediated growth remains a challenging task. In this work, we implement and analyze gold nanorods growth and etching processes in the presence of gold salts when irradiated with femtosecond laser pulses (fs) which are particularly favorable to so-called hot electron processes. Indeed, this regime of ultrashort fs impulsions generates hot carriers in high yield in the gold NR.[13] These highly energetic photogenerated carriers adopt a spatial distribution closely related to the modal distribution of theses plasmonic resonators and thus, for a given excitation energy, initiate various processes, including gold overgrowth and etching, with a distinct spatial pattern.[7,13–16] Here, the LSPR wavelength, initially 800nm, is used to promote anisotropic hot carrier generation through plasmon-enhanced two-photon absorption within NRs. On the contrary, gold interband transition is exploited to directly absorb 400nm photons and generate isotropic hot carriers and heating. We describe here a series of exper-

iments that mitigate this point of view and allow us to discuss the underlying photophysical and/or photochemical processes. We show first that tips of Au NR irradiated at 800 nm in the presence of free $AuCl_4^-$ are selectively etched, while irradiation at 400 nm promotes uniform and isotropic growth of both tips and sides (figure 1.a). A purpose-designed UV-Vis spectrometer triggered by the femtosecond pulsed laser allowed us to monitor *in situ* and in realtime the photochemical reactions. These spectral observations are compared to post-synthesis transmission electron microscopy images and to 3D electromagnetic simulations. When the fs irradiation wavelength is tuned to 400 nm, the free gold ions are photoactivated and contribute to the NR growth. In contrast, coupling the laser irradiation to the LSPR has a markedly different effect since it results in a site-specific etching of the NR tips.

Materials and methods

Preparation of the irradiated solutions

All chemicals were bought from commercial suppliers. CTAB-coated gold nanorods (LPSR, 808 nm, [CTAB], 5 mM) were purchased from Nanopartz (Loveland, CO). Tetrachloroauric acid ($HAuCl_4 \cdot 3H_2O$) was purchased from Sigma Aldrich. In order to conduct irradiation experiments in which spontaneous tip etching of Au NR by $AuCl_4^-$ is negligible and thus focus on the effect of the fs laser alone, CTAB concentration was reduced below critical micelle concentration.[17]

To avoid tip etching, 1000 µL of Au NR colloids were centrifuged at 12,000 relative centrifugal force (rcf) for 4 minutes and 30 seconds. 95% of the supernatant was removed, and the remaining solution was redispersed in 450 µL of deionized water. A portion of 180 µL of the solution was taken, and 20 µL of 1 mM chloroauric acid solution was added. The sample was transferred into a microcuvette (Thorlabs, CV10Q1FE) and left to equilibrate for 30 minutes prior to femtosecond laser irradiation and characterization.

Irradiation and characterization

The $AuCl_4^-$-NR solutions were irradiated with a tunable Ti:Sapphire femtosecond laser with a pulse duration of 120 fs and a repetition rate of 80 MHz. The excitation wavelength was 800 nm corresponding to the longitudinal surface plasmon resonance (LSPR) wavelength or 400 nm by using the Second Harmonic Generation of the femtosecond laser through a nonlinear crystal. The laser beam is expanded employing a diverging lens (f=10 cm) placed 50 cm before the cuvette containing the NR solution to ensure uniform illumination, resulting in a final irradiance of 2.65×10^6 mW cm^{-2}/pulse. During laser illumination, we probed the absorption spectra of the solution in order to follow dynamically the changes of the SPR resonances (both LSPR and TSPR) using a compact CCD spectrometer (Thorlabs, CCS200) with a tungsten light source (Thorlabs, SLS202L). All absorption spectra measurements started several minutes before irradiation to check the solution stability without laser. During the femtosecond irradiation, the light scattered by the NR saturates the CCD sensor of the spectrometer. To avoid this problem, the spectra acquisition was triggered by a shutter blocking the laser beam. For each cycle of measurement the shutter remains open for 10 s and closed for 1 s. A scheme of the experiment is shown in figure 1.b.

Results

Typical initial absorption spectra of the NR solution with and without added free $AuCl_4^-$ ions are shown in figure 2.a. Figure 2.b shows the observed spectra after 30 min of irradiation at either 400 nm or 800 nm wavelength irradiation. When a wavelength of 400 nm was used, the longitudinal surface plasmon resonance (LSPR) undergoes a sizeable blue shift, the optical density of both plasmon resonances increases but the absorption band associated to the free $AuCl_4^-$ ions (below 500nm) is reduced. Irradiation at 800 nm also results in a blue shift but a marked decrease of the OD at the LSPR wavelength is observed along with an increase in the spectral region associated with the free Au(III) ions. The *in situ* real time

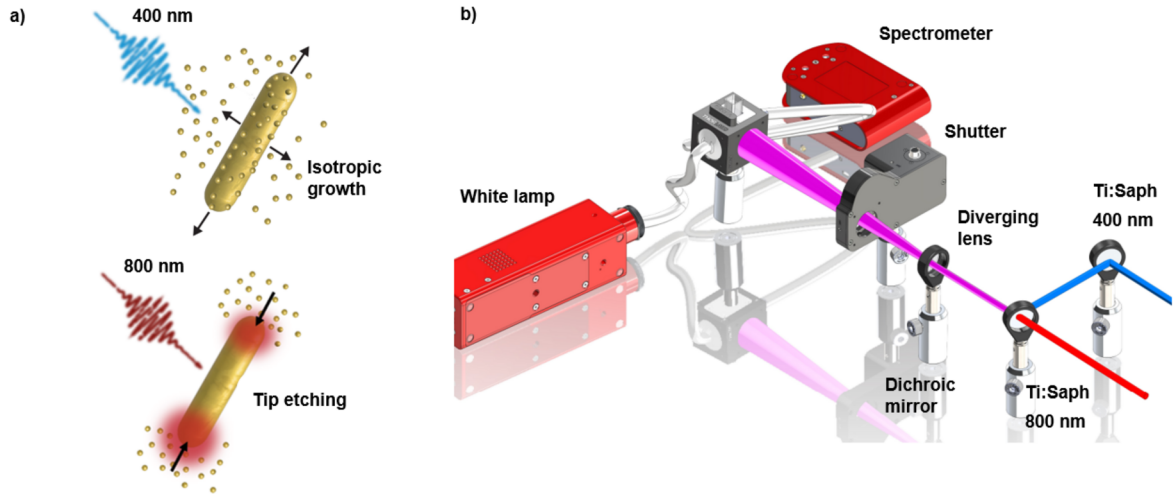

Figure 1: a) Schematics illustrating the wavelength-dependent reshaping of Au NR in the presence of $AuCl_4^-$ and femtosecond irradiation. Illumination at 400 nm causes adsorption of atoms over the entire NR surface, resulting in isotropic growth. Under illumination at 800 nm, matching the longitudinal surface plasmon resonance (LSPR), desorption of atoms occurs specifically at the tips of the NR, leading to selective etching . b) Schematic illustrating the experimental setup used in this work. The solution containing Au nanorods is irradiated with a tunable femtosecond laser while the UV-Vis absorption spectrum is monitored in real-time.

evolution of these spectral changes during the entire irradiation experiment are displayed in the colormaps presented in Figure 2.c and 2.d. With regard to the kinetics of the evolution of the photo-induced reactions observed, we notice a direct dependence of the evolution rate of the solutions on the laser power, i.e. the higher the laser power, the faster the evolution rate. The laser power used in the experiments reported here represents our best compromise in terms of experiment duration, acquisition rates and stability of experimental parameters (see Materials and Methods).

Subsequently, transmission electron microscopy (TEM) observations (shown in figure 3.a) were conducted to assess the size distribution of the NR before and after laser irradiation. A statistical analysis of each particle size distribution was conducted using IJ Blob19,[18] an automated particle recognition and sizing algorithm, from the TEM images of several hundreds of NR. The resulting two-dimensional histograms are shown in figure 3.b and consist in a single oblong data cloud along with an AR shift from AR=4.1 to AR=3.6

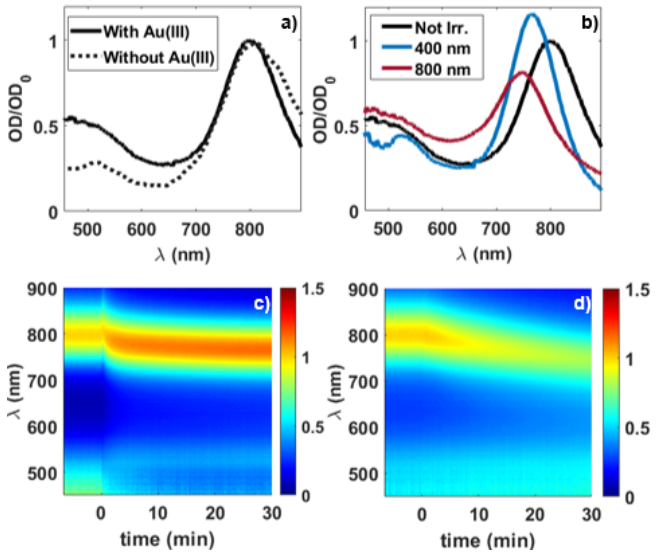

Figure 2: a) Absorption spectra of a typical NR colloid before and after $AuCl_4^-$ addition. b) Comparison of the final spectra obtained under 800 nm, 400 nm irradiation and without irradiation. Spectrogram showing the evolution of Au NR absorption spectrum under femtosecond irradiation at 800 nm (c) and 400 nm (d).

after irraditation at 400 nm and to AR=2.7 after irradiation at 800 nm. More precisely, we observe that the NR grow both in width and length upon irradiation at 400 nm, while they undergo uniaxial tip etching without any significant change in width when 800 nm irradiation is used (illustration figure 3.c). We also note that the irradiated solutions have a higher polydispersity than the initial solution and this could probably be improved in future work. Nevertheless, the trends observed remain sufficiently clear to support our conclusions, which are also confirmed by the analyzis of the measured and simulated absorption spectra shown hereafter.

As any morphological change (in surface or volume) induces a change in the effective absorption and scattering cross-sections of the rods, we numerically determine these quantities from the dimensions of the rods measured by TEM, also taking into account their size dispersion. We used the Green Dyadic Method and its open-source python implementation pyGDM[19] to compute the absorption spectrum of each NR population shown in figure 3. First, we calculate the extinction cross section of single gold NR of width w and length l in

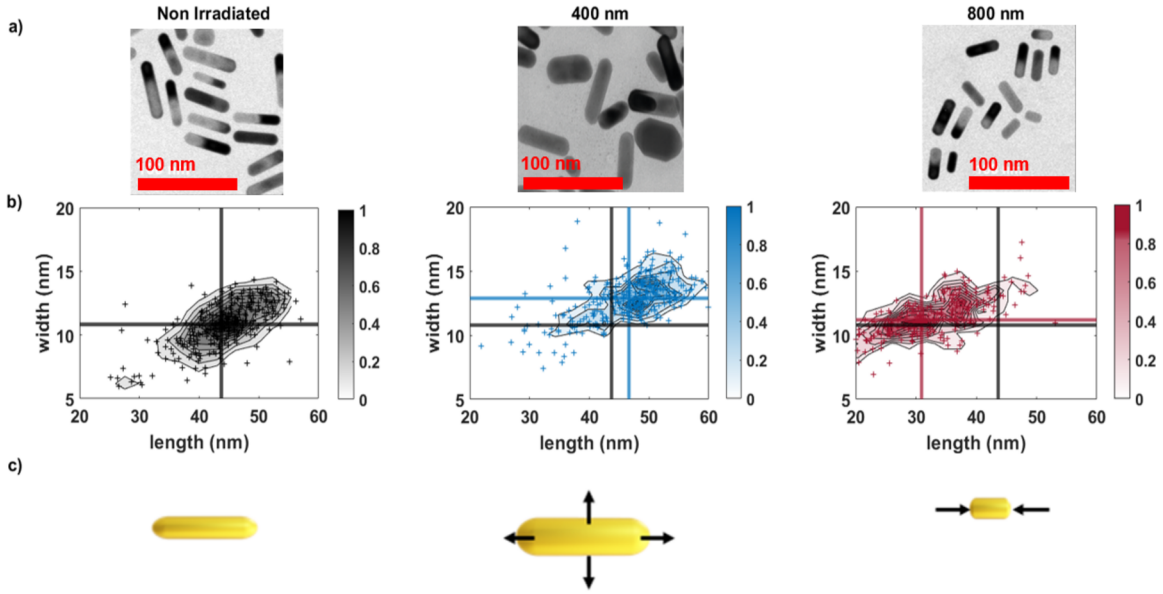

Figure 3: a) Typical TEM images of the NR before and after irradiation at 400nm and 800nm. b) 2D histograms of length, width of Au NR before and after irradiation. Black cursor shows the average length and width in the non irradiated solution. Blue and red cursor respectively represent the averages at 400 nm and 800nm. The colorbars represent the normalized density of NR of a given length and width. The average AR are shown in insets. Number of NR analyzed for each condition: $N_{NI} = 307$, $N_{400\,\mathrm{nm}} = 306$, and $N_{800\,\mathrm{nm}} = 295$, c) Illustration of the isotropic growth and tip etching when the NR are respectively irradiated at 400 nm and 800 nm

.

water ($n = 1.33$). NR are illuminated by a linearly polarized incident plane wave with the electric field aligned either along its longitudinal axis or along its transverse axis in order to excite independently the LSPR or TSPR mode respectively. If we consider the suspension as a disordered ensemble of non-interacting nanorods, the averaged extinction cross section can be modeled from a statistical morphological distribution provided in figure 3 and an extinction cross section of an individual, randomly oriented ellipsoidal NR. Indeed, the shape effect on a single NR assimilated to a prolate ellipsoide is well described by a simple diagonal anisotropic polarizability tensor.[20] The extinction cross section of a single randomized oriented nanorod is then given by equation 1.

$$\sigma_{w,l}(\lambda) = [2\sigma^{\perp}_{w,l}(\lambda) + \sigma^{\parallel}_{w,l}(\lambda)]/3 \tag{1}$$

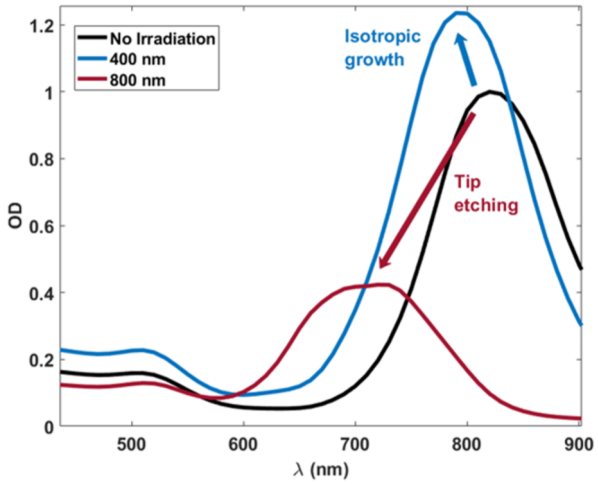

Figure 4: Simulated absorption spectra of NR colloids using TEM size distributions for the non-irradiated colloid (black), after the 400nm irradiation (blue) and after 800nm irradiation (red).

where $\sigma_{w,l}$ is the extinction cross section of a NR of width w and length l, $\sigma_{w,l}^{\perp}$ its transverse extinction cross section and $\sigma_{w,l}^{\parallel}$ its longitudinal one. The averaged extinction cross section, $\sigma(\lambda)$, is obtained by weighting $\sigma_{w,l}(\lambda)$ by the statistical distribution of the dimensional measurements from TEM images shown in figure 3.b and represented by the two-dimensional probability density function, $P(w,l)$ as shown in equation 2.

$$\sigma(\lambda) = \Sigma_{w,l}\sigma_{w,l}(\lambda)P(w,l) \tag{2}$$

The calculated absorption spectra are shown in figure 4 and demonstrate that the isotropic growth under 400 nm irradiation results in a slight blue shift of the LSPR resonance and an increase of the OD. The tip etching observed at 800 nm irradiation also leads to a blueshift of the LSPR but with an overall decrease in OD. Additionnaly, the TSPR wavelength remains unchanged but its OD is increased for NR after 400 nm illumination. These numerical results are thus in good agreement with UV-Vis absorption spectroscopy observations and consistent with the literature that links the NR AR and their absorption spectra.[3–8,21,22] In spite of a good qualitative agreement, our electromagnetic simulations do not take into account the time-evolving contribution of the free $AuCl_4^-$ ions observed experimentally. We adress this

point hereafter.

Discussion

The femtosecond laser illumination of the suspension of gold nanorod resonators clearly results in a marked reshaping of the gold nanostructures. The reported wavelength dependency that switches the reshaping from etching to overgrowth can not be explained by a direct melting of the NR under intense irradiation such as in[23] where a high power density ($3J/m^2$) was employed. Moreover the photosensitive evolution of the free $AuCl_4^-$ ion concentration suggest that more complex underlying photochemical processes are on-going. In recent works, Au overgrowth and etching have been attributed to photogenerated hot carriers induced by reduction of $AuCl_4^-$ at the vicinity of the NR.[7,15,16,24] Here, at 400 nm, hot electrons are directly generated by linear absorption and 5d to 6sp interband transition. The resulting homogeneous hot electron density within the NR could, in turn, trigger the observed isotropic growth by reduction of vicinal free $AuCl_4^-$ ions. However, 800 nm irradiation only indirectly promotes hot electrons generation through a plasmon enhanced multiphoton absorption process.[13] The corresponding anisotropic hot electron distribution within the NR reflects the plasmon modal distribution with a maximal concentration of carriers at the tip of the NR where the electromagnetic field is enhanced. As such, 800 nm irradiation should trigger an anisotropic growth confined at the NR tips when we observed a tip etching. The reported results can therefore not be attributed solely to hot carriers catalysis of gold ions which raises two questions: (i) Is there any direct interaction between the femtosecond laser pulses and the solution itself? (ii) What is the role of the LSPR-laser coupling in the reported experiment at 800 nm?

To answer the first question, the previous experiments were repeated with the same conditions but without NR. $AuCl_4^-$ solutions prepared at the same concentration were irradiated for 1 hour at either 400 or 800nm wavelengths under gentle stirring. The UV-Vis absorption spectra of the initial and irradiated solutions are shown in figure 5.a. The initial solution is

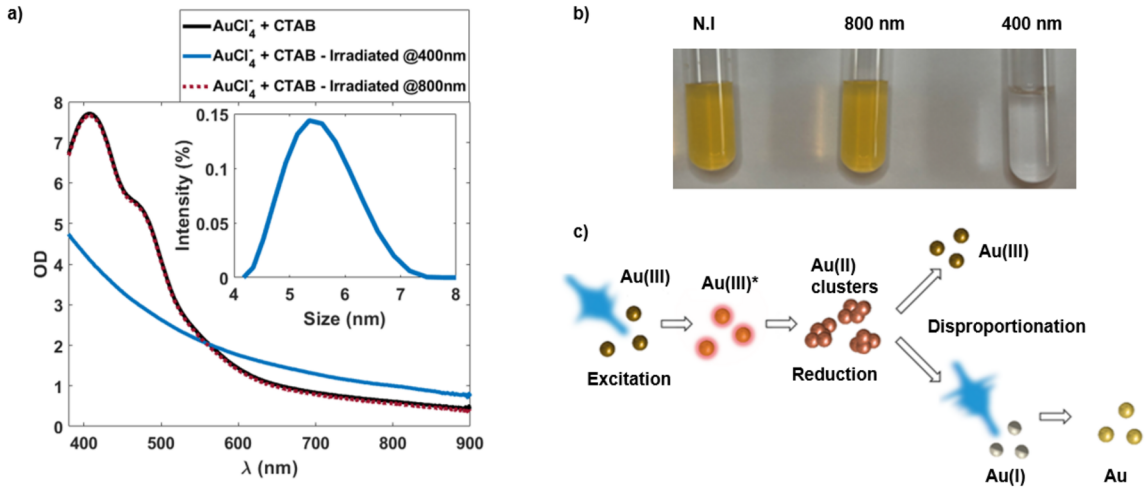

Figure 5: a) Absorption spectra of irradiated and unirradiated $AuCl_4^-$ solutions without NR. Inset shows DLS sizing measurement for 400nm irradiation. b) Photographs of the $AuCl_4^-$ solutions before and after irradiation at both wavelengths. c) Schematics of the proposed mechanism for $AuCl_4^-$ photoreduction under 400 nm irradiation.

clear and yellowish and exhibits two absorption peaks at 405 nm and 471 nm, which suggest the formation of a Au(III)-CTAB complexes.[25] Irradiation with the 800 nm wavelength does not change any spectral feature of the solution and spectra before and after irradiation are almost perfectly superimposed. On the contrary, upon 400 nm irradiation, the solution appearance turns immediately colorless (see photographs in figure 5.b) and becomes slightly turbid, which can be observed with the naked eye in the laboratory but is difficult to observe from the photo. The absorption spectrum no longer shows the two absorption peaks of Au(III)-CTAB complex but rather the typical Rayleigh scattering of a small nanoparticles. Note that no plasmon resonance band emerges in these irradiation conditions. Dynamic light scattering (DLS) measurements conducted on the different solutions are shown in the inset of figure 5.a and reveal the presence of nanospheres of 5 nm to 6 nm hydrodynamic diameter only for irradiation at 400nm. Therefore, these observations indicate the photo reduction of $AuCl_4^-$ and the formation of sub-plasmonic metallic Au clusters when solution is irradiated at 400nm. In contrast to earlier reports on the reduction of Au(III) ions by multiphoton absorption, the energy density used in our conditions is ten to twelve orders of magnitude lower: 10^{16} W cm^{-2} to 10^{18} W cm^{-2}/pulse in[26–28] versus 2.65×10^6 W cm^{-2}/pulse

in our case. It is therefore unlikely that the mechanism of Au(III) reduction mediated by water photolysis invoked in these studies also applies here. An alternative interpretation, proposed by Kurihara *et al.*,[29] consists in a multistep photochemical mechanism for the conversion of $AuCl_4^-$ to Au(0) as depicted in figure 5.c. Upon UV photon absorption, excited $AuCl_4^-$ decays into oxidized Cl(0) and transient caged $AuCl_2^-$ complexe,[30] which is highly unstable and rapidly disproportionate into $AuCl_4^-$ and $AuCl_2^-$. Monovalent Au ions are then reduced upon further UV photon absorption and Cl(0) release.[29] In the absence of NR, the second step of photoinduced reduction into Au(0) results in the formation of small metallic gold nanoparticles as observed in figure 5.a. When NR are present in the solution, this reduction is promoted by the catalytic activity of partially reduced gold atoms on the NR surface, therefore feeding the isotropic morphological evolution of the NR observed for irradiation at 400nm.

On the contrary, 800nm irradiation does not directly interact with the $AuCl_4^-$-CTAB solution which necessarily implies a contribution of NR properties in the reported results. Hence, to get insight in the laser-LSPR coupling, analyze the contribution of absorbed laser power on the observed process and answer the second question above, the reaction evolution rate is measured as a function of the laser power instantaneously absorbed by the LSPR. The initial LSPR wavelength at 800 nm prompted us to irradiate the suspension at 800 nm for 30 min and examine the impact of the laser-LSPR coupling on the kinetics of the ongoing reactions by recording, *in situ*, the changes of absorption spectrum. The recorded time evolution of the absorption spectrum is shown in figure 6.a. The LSPR blue-shift gradually decreases the overlap between plasmonic resonance and the excitation laser wavelength. Thus, as the reaction proceeds, the LSPR excitation efficiency is reduced, which, in turn, slows down the photoinduced and plasmon-mediated reactions. The amount of laser power actually coupled to the LSPR and absorbed, P_{abs}, can be estimated by weighting the laser

power, P_{Laser}, by the solution absorbance at the laser wavelength, λ, as given by equation 3:

$$P_{\text{abs}} = (1 - 10^{-\text{OD}_\lambda(t)})P_{\text{Laser}} \tag{3}$$

where $\text{OD}_\lambda(t)$ is the instantaneous OD due to the LSPR absorption at the laser wavelength.

The time evolution of P_{abs} is shown in figure 6a. Since all TEM analysis show that the gold nanostructures remain well-separated nanorods during the entire process, the LSPR blue shift probes the evolution of the NR AR or, rather, the evolution of the NR length since their width remains unmodified (See figure 3.a, 800 nm). In figure 6.b in red, we therefore extract time derivative of the LSPR wavelength from the absorption spectra, $d\lambda_{LSPR}/dt$, as a representative assessement of the tip etching rate kinetics.

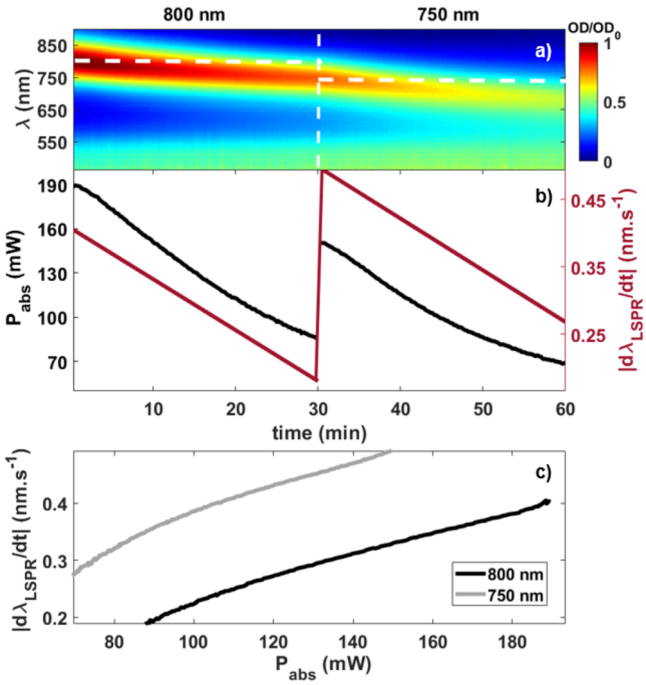

Figure 6: a) Colormap showing the evolution of the absorption spectra recorded during the experiment. The laser was turned on at $t = 0$ s and its wavelength was tuned to the new LPSR resonance at $t = 30$ min. b) Absorbed power versus time calculated from the absorption spectra and using equation 2 c) Derivative of the LSPR wavelength versus the absorbed power for the two sequences of the irradiation.

As the suspension is irradiated at 800 nm for the first 30 min, the absorbed power de-

creases linearly. Concommittantly, the LSPR blue shifts but the shift rate decreases with a similar time evolution as the absorbed power. The slightly non-linear time evolution of the LPSR shift can be attributed to diffusion limited availability of free Au(III) ions near the NR surface. Interestingly, when the laser wavelength is re-tuned in registry with the modified LSPR wavelength at t=30 mn, the LSPR blue shift rate increases instantaneously with the absorbed power. Then again, the LSPR wavelength blueshifts with a gradually decreasing kinetics that matches the linearly decreasing absorbed power evolution with the small non-linear contribution previously observed.

Additionally, matching the running LSPR resonance wavelength with the excitation laser wavelength allows to post-synthetically tune the NR length by more than 130 nm (from 805 to 670 nm), i.e. by more than 45% of possible reshaping range from NR to spherical nanoparticle. Finally, figure 6.c presents $d\lambda_{LSPR}/dt$ versus $P_{\text{abs}}(t)$, which provides the relationship between the reaction kinetics and the laser power actually absorbed by the NR. Linear relationship between these quantitities for both irradiation wavelengths shows that the reaction kinetics is driven by LSPR excitation. Tip etching rate becoming maximum as LSPR is excited with the best efficiency, this represents a direct demonstration of the plasmonic resonance photocatalytic effect. Note that tip etching rate for 750nm irradiation is twice faster than for 800nm irradiation for the same $P_{\text{abs}}(t)$. This may be due either to an increase in the density of electrons photogenerated and harvested deeper in the -d bands because of a higher excitation energy, or to a strengthening of the local field at the tips of the NR due to an increasingly pronounced antenna effect as LSPR is shifted towards the visible. In both cases, NR electronic relaxation turns into local heating of the nanoparticle which could also favor the oxidative etching rate of nanorods tips in presence of $AuCl_4^-$ and CTAB as reported in.[17] However, distinguishing between hot electron processes and thermal effects remains a challenge and would require advanced pump-probe experiments after identifying the appropriate optical quantities to control in order to access the instantaneous temperature of nanoparticles. This would probably close the debate concerning the contributions of hot

electrons versus thermal effects in plasmonic-mediated photocatalysis, but is well beyond the scope of this work.

Conclusion

In conclusion, we reported here on the post-synthesis gold nanorods growth and etching under femtosecond irradiation in presence of $AuCl_4^-$. We conducted a series of optical experiments combined to TEM analysis and numerical modeling to unveil the underlying photochemical mechanisms. We established that blue irradiation promotes gold overgrowth through direct photoreduction of gold ions in solution and without contribution of the nanoparticles properties. In contrast, near infrared irradiation promotes a selective gold oxidative etching driven by surface plasmon resonance excitation. As such, the results reported in this paper provides new insights into the active field of plasmonic photocatalysis[31] and will feed the debate on the underlying photo-induced mechanisms.[32–35] As the proposed approach allows the fine tuning of the the LSPR wavelength across a broad spectral range, this may also find application in the fields of plasmonic colors,[36] sensors,[37,38] or absorbers[39] where a post-synthesis or post-fabrication control on the absorption-to-scattering ratio is highly desirable.

Acknowledgement

This work benefited from the facilities of the SMARTLIGHT platform (EQUIPEX+ contract "ANR-21-ESRE-0040"). It has been supported by the EIPHI Graduate School (contract "ANR-17-EURE-0002") Région Bourgogne Franche-Comté, and the ANR RANDOM project (contract "ANR-19-CE24-0014"). We thank DImaCell Platform, AgroSup Dijon, INRA, Univ. Burgundy Franche-Comté, F-21000 Dijon, France for allowing the access to the Transmission Electronic Microscope.

References

(1) Li, N.; Zhao, P.; Astruc, D. Anisotropic Gold Nanoparticles: Synthesis, Properties, Applications, and Toxicity. *Angewandte Chemie International Edition* **2014**, *53*, 1756–1789.

(2) Méjard, R.; Verdy, A.; Demichel, O.; Petit, M.; Markey, L.; Herbst, F.; Chassagnon, R.; Colas-des Francs, G.; Cluzel, B.; Bouhelier, A. Advanced engineering of single-crystal gold nanoantennas. *Optical Materials Express* **2017**, *7*, 1157–1168, Publisher: Optica Publishing Group tex.copyright: © 2017 Optical Society of America.

(3) Khanadeev, V. A.; Khlebtsov, N. G.; Burov, A. M.; Khlebtsov, B. N. Tuning of plasmon resonance of gold nanorods by controlled etching. *Colloid Journal* **2015**, *77*, 652–660.

(4) Ni, W.; Kou, X.; Yang, Z.; Wang, J. Tailoring Longitudinal Surface Plasmon Wavelengths, Scattering and Absorption Cross Sections of Gold Nanorods. *ACS Nano* **2008**, *2*, 677–686.

(5) Thambi, V.; Kar, A.; Ghosh, P.; Khatua, S. Light-Controlled in Situ Bidirectional Tuning and Monitoring of Gold Nanorod Plasmon via Oxidative Etching with FeCl . *The Journal of Physical Chemistry C* **2018**, *122*, 24885–24890.

(6) Khlebtsov, B. N.; Khanadeev, V. A.; Ye, J.; Sukhorukov, G. B.; Khlebtsov, N. G. Overgrowth of Gold Nanorods by Using a Binary Surfactant Mixture. *Langmuir : the ACS journal of surfaces and colloids* **2014**, *30*, 1696–1703.

(7) Forcherio, G. T.; Baker, D. R.; Boltersdorf, J.; Leff, A. C.; McClure, J. P.; Grew, K. N.; Lundgren, C. A. Targeted Deposition of Platinum onto Gold Nanorods by Plasmonic Hot Electrons. *The Journal of Physical Chemistry C* **2018**, *122*, 28901–28909.

(8) Ratto, F.; Matteini, P.; Rossi, F.; Pini, R. Size and shape control in the overgrowth of gold nanorods. *Journal of Nanoparticle Research* **2010**, *12*, 2029–2036.

(9) Lohse, S. E.; Murphy, C. J. The Quest for Shape Control: A History of Gold Nanorod Synthesis. *Chemistry of Materials* **2013**, *25*, 1250–1261.

(10) John, C. L.; Strating, S. L.; Shephard, K. A.; Zhao, J. X. Reproducibly synthesize gold nanorods and maintain their stability. *RSC Advances* **2013**, *3*, 10909.

(11) Burrows, N. D.; Harvey, S.; Idesis, F. A.; Murphy, C. J. Understanding the Seed-Mediated Growth of Gold Nanorods through a Fractional Factorial Design of Experiments. *Langmuir : the ACS journal of surfaces and colloids* **2017**, *33*, 1891–1907, Publisher: American Chemical Society.

(12) Scarabelli, L.; Sánchez-Iglesias, A.; Pérez-Juste, J.; Liz-Marzán, L. M. A "Tips and Tricks" Practical Guide to the Synthesis of Gold Nanorods. *The Journal of Physical Chemistry Letters* **2015**, *6*, 4270–4279.

(13) Demichel, O.; Petit, M.; Viarbitskaya, S.; Méjard, R.; De Fornel, F.; Hertz, E.; Billard, F.; Bouhelier, A.; Cluzel, B. Dynamics, Efficiency, and Energy Distribution of Nonlinear Plasmon-Assisted Generation of Hot Carriers. *ACS Photonics* **2016**, *3*, 791–795.

(14) Minutella, E.; Schulz, F.; Lange, H. Excitation-Dependence of Plasmon-Induced Hot Electrons in Gold Nanoparticles. *The Journal of Physical Chemistry Letters* **2017**, *8*, 4925–4929, Publisher: American Chemical Society.

(15) Zhao, J.; Nguyen, S. C.; Ye, R.; Ye, B.; Weller, H.; Somorjai, G. A.; Alivisatos, A. P.; Toste, F. D. A Comparison of Photocatalytic Activities of Gold Nanoparticles Following Plasmonic and Interband Excitation and a Strategy for Harnessing Interband Hot Carriers for Solution Phase Photocatalysis. *ACS Central Science* **2017**, *3*, 482–488.

(16) Long, Y.; Wang, S.; Wang, Y.; Deng, F.; Ding, T. Light-Directed Growth/Etching of Gold Nanoparticles via Plasmonic Hot Carriers. *The Journal of Physical Chemistry C* **2020**, *124*, 19212–19218.

(17) Rodríguez-Fernández, J.; Pérez-Juste, J.; Mulvaney, P.; Liz-Marzán, L. M. Spatially-Directed Oxidation of Gold Nanoparticles by Au(III)-CTAB Complexes. *The Journal of Physical Chemistry B* **2005**, *109*, 14257–14261.

(18) IJBlob: An ImageJ Library for Connected Component Analysis and Shape Analysis. *Journal of Open Research Software* **2013**, *1*, e6.

(19) Wiecha, P. R. pyGDM – A python toolkit for full-field electro-dynamical simulations and evolutionary optimization of nanostructures. *Computer Physics Communications* **2018**, *233*, 167–192, arXiv: 1802.04071.

(20) Dujardin, E.; Girard, C. In *Handbook of Nanophysics, Nanoparticles and Quantum Dots*, 0th ed.; Sattler, K. D., Ed.; CRC Press, 2016; pp 471–496.

(21) Cavigli, L.; Khlebtsov, B. N.; Centi, S.; Khlebtsov, N. G.; Pini, R.; Ratto, F. Photostability of Contrast Agents for Photoacoustics: The Case of Gold Nanorods. *Nanomaterials* **2021**, *11*, 116.

(22) Kermanshahian, K.; Yadegar, A.; Ghourchian, H. Gold nanorods etching as a powerful signaling process for plasmonic multicolorimetric chemo-/biosensors: Strategies and applications. *Coordination Chemistry Reviews* **2021**, *442*, 213934.

(23) González-Rubio, G.; Díaz-Núñez, P.; Rivera, A.; Prada, A.; Tardajos, G.; González-Izquierdo, J.; Bañares, L.; Llombart, P.; Macdowell, L. G.; Alcolea Palafox, M. et al. Femtosecond laser reshaping yields gold nanorods with ultranarrow surface plasmon resonances. *Science* **2017**, *358*, 640–644.

(24) Guo, W.; Johnston-Peck, A. C.; Zhang, Y.; Hu, Y.; Huang, J.; Wei, W. D. Cooperation of Hot Holes and Surface Adsorbates in Plasmon-Driven Anisotropic Growth of Gold Nanostars. *Journal of the American Chemical Society* **2020**, *142*, 10921–10925.

(25) Anandhakumar, S.; Rajaram, R.; Mathiyarasu, J. Unusual seedless approach to gold nanoparticle synthesis: Application to selective rapid naked eye detection of mercury(II). *The Analyst* **2014**, *139*, 3356–3359, Publisher: The Royal Society of Chemistry.

(26) Moore Tibbetts, K.; Tangeysh, B.; Odhner, J. H.; Levis, R. J. Elucidating Strong Field Photochemical Reduction Mechanisms of Aqueous [AuCl] : Kinetics of Multiphoton Photolysis and Radical-Mediated Reduction. *The Journal of Physical Chemistry A* **2016**, *120*, 3562–3569.

(27) Nakamura, T.; Mochidzuki, Y.; Sato, S. Fabrication of gold nanoparticles in intense optical field by femtosecond laser irradiation of aqueous solution. *Journal of Materials Research* **2008**, *23*, 968–974, Publisher: Cambridge University Press.

(28) Inasawa, S.; Sugiyama, M.; Koda, S. Size Controlled Formation of Gold Nanoparticles Using Photochemical Grwoth and Photothermal Size Reduction by 308 nm Laser Pulses. *Japanese Journal of Applied Physics* **2003**, *42*, 6705–6712.

(29) Kurihara, K.; Kizling, J.; Stenius, P.; Fendler, J. H. Laser and pulse radiolytically induced colloidal gold formation in water and in water-in-oil microemulsions. *Journal of the American Chemical Society* **1983**, *105*, 2574–2579.

(30) Eustis, S.; Hsu, H.-Y.; El-Sayed, M. A. Gold Nanoparticle Formation from Photochemical Reduction of Au ^{3} by Continuous Excitation in Colloidal Solutions. A Proposed Molecular Mechanism. *The Journal of Physical Chemistry B* **2005**, *109*, 4811–4815.

(31) Cortés, E.; Besteiro, L. V.; Alabastri, A.; Baldi, A.; Tagliabue, G.; Demetriadou, A.; Narang, P. Challenges in Plasmonic Catalysis. *ACS Nano* **2020**, *14*, 16202–16219, Publisher: American Chemical Society.

(32) Dubi, Y.; Sivan, Y. "Hot" electrons in metallic Nanostructures—Non-Thermal carriers

or heating? *Light: Science & Applications* **2019**, *8*, 89, Publisher: Nature Publishing Group tex.copyright: 2019 The Author(s).

(33) Baffou, G.; Bordacchini, I.; Baldi, A.; Quidant, R. Simple experimental procedures to distinguish photothermal from hot-carrier processes in plasmonics. *Light: Science & Applications* **2020**, *9*, 108, Publisher: Nature Publishing Group tex.copyright: 2020 The Author(s).

(34) Jain, P. K. Taking the Heat Off of Plasmonic Chemistry. *The Journal of Physical Chemistry C* **2019**, *123*, 24347–24351.

(35) Jain, P. K.; Qian, W.; El-Sayed, M. A. Ultrafast Cooling of Photoexcited Electrons in Gold Nanoparticle-Thiolated DNA Conjugates Involves the Dissociation of the Gold-Thiol Bond. *Journal of the American Chemical Society* **2006**, *128*, 2426–2433.

(36) Wang, X.; Xu, D.; Jaquet, B.; Yang, Y.; Wang, J.; Huang, H.; Chen, Y.; Gerhard, C.; Zhang, K. Structural Colors by Synergistic Birefringence and Surface Plasmon Resonance. *ACS Nano* **2020**, *14*, 16832–16839, Publisher: American Chemical Society.

(37) Becker, J.; Trügler, A.; Jakab, A.; Hohenester, U.; Sönnichsen, C. The Optimal Aspect Ratio of Gold Nanorods for Plasmonic Bio-sensing. *Plasmonics* **2010**, *5*, 161–167.

(38) Li, J.; Wei, Y.-Y.; Liu, X.-P.; Xu, Z.-R. Plasmonic photothermal biosensor for visual detection of tyrosinase and dopamine based on manganese dioxide nanosheets-mediated etching of gold nanorods. *Sensors and Actuators B: Chemical* **2022**, *353*, 131139.

(39) Shu, Y.; Guo, P.; Li, X.; Li, G.; Wang, P.; Shen, G.; Li, J. Gold Nanorods as Saturable Absorber for Harmonic Soliton Molecules Generation. *Frontiers in Chemistry* **2019**, *7*, 715.